Energy-dependent evolution of ring current protons during magnetic storms

Ayako Temporin[1] and Yusuke Ebihara[2]

Received 25 March 2011; revised 29 August 2011; accepted 30 August 2011; published 1 October 2011.

[1] The storm time evolution of equatorially mirroring H^+ ions in the inner magnetosphere has been statistically examined by using data from the Polar satellite. We focused on two energy ranges of H^+ observed by Polar; 31–80 keV and 125–173 keV, which are referred to as low- and high-energy components, respectively. The following two phases were defined; the developing phase (pre-storm time to near the most disturbed time) and the declining phase (near the most disturbed time to post-storm time), which is 3 days before (after) the equatorial crossing of Polar during the storm time. We obtained the following results: (1) Low-energy H^+ tends to increase during the developing, and to decrease during the declining at all magnetic local times (MLTs) except for the pre-noon sector. (2) The low-energy H^+ is anti-correlated with the magnetic field, probably indicating that the low-energy H^+ reduces the equatorial magnetic field due to a diamagnetic effect. (3) High-energy H^+ tends to increase on the dayside during the declining phase. (4) The high-energy H^+ is poorly correlated with the magnetic field. High-energy H^+ behaves significantly different from the low-energy H^+, and that some process other than betatron acceleration, diffusion and substorm-associated injection could have been responsible for the variation of the high-energy H^+.

Citation: Temporin, A., and Y. Ebihara (2011), Energy-dependent evolution of ring current protons during magnetic storms, *J. Geophys. Res.*, *116*, A10201, doi:10.1029/2011JA016692.

1. Introduction

[2] The ring current flows at radial distances of several earth radii, and is significantly enhanced during magnetic storms [e.g., *Smith and Hoffman*, 1974; *Lui et al.*, 1987]. All of the trapped particles contribute to the ring current, but in particular, ions with energy ranging from ~10 keV to a few hundreds of keV are thought to be dominant contributors to the ring current [e.g., *Frank*, 1967; *Williams*, 1987]. Electrons contribute little to the ring current on account of their negligible energy density [*Liu et al.*, 2005]. The ring current globally modifies the distributions of the ground magnetic field known as the *Dst* index [e.g., *Cahill*, 1966] and in the inner magnetosphere [e.g., *Hoffman and Cahill*, 1968; *Berko et al.*, 1975; *Krimigis et al.*, 1985]. The modified magnetic field can redistribute the particles contributing to the ring current [e.g., *Lyons and Williams*, 1976; *Fu et al.*, 2001; *Zaharia et al.*, 2005; *Ebihara et al.*, 2008] and the radiation belt [e.g., *Dessler and Karplus*, 1961; *McIlwain*, 1966; *Williams et al.*, 1968; *Li et al.*, 1997; *Shprits et al.*, 2006].

[3] Satellite observations have shown that the energy distribution of the H^+ ions depends on magnetic activities and the phase of magnetic storms. During quiet times, the ring current is dominated by H^+ ions in the energy range from 100 keV to several hundreds of keV [*Krimigis et al.*, 1985]. During a storm main phase, ions with energy ranging between several keV and several tens of keV become dominant [e.g., *Frank*, 1967; *Smith and Hoffman*, 1973; *Lyons and Williams*, 1976; *Williams*, 1981; *Krimigis et al.*, 1985; *Fu et al.*, 2001], whereas ions with energy greater than 100 keV show an abrupt decrease [*Lyons and Williams*, 1976; *Lyons*, 1977; *Williams*, 1981; *Fu et al.*, 2001]. During a storm recovery phase, ions with energy ranging between several keV and several tens of keV show a decrease, whereas ions with energy greater than 100 keV show an increase [*Lyons and Williams*, 1976; *Fu et al.*, 2001]. These observational facts clearly show opposite tendencies for ions with energy less than several tens of keV and greater than 100 keV.

[4] *Lyons* [1977] has explained the decrease (increase) in ions with energy greater than 200 keV in terms of adiabatic deceleration (acceleration) of the ions. As the ring current develops, the equatorial magnetic field is decreased (inflated) by the ring current. The decrease (inflation) of the equatorial magnetic field can decelerate trapped particles, resulting in the development of large minima at 90° in the equatorial pitch angle distributions due to the conservation of the first adiabatic invariant. *Ebihara et al.* [2008] have demonstrated that during the large magnetic storm of 22 October 1999, H^+ flux at 80–173 keV was decreased at pitch angles near 90°, whereas increased at pitch angles near 0° and 180° near the equatorial plane at $L \approx 5$. The decrease and increase in the H^+

[1]Solar-Terrestrial Environment Laboratory, Nagoya University, Nagoya, Japan.
[2]Research Institute for Sustainable Humanosphere, Kyoto University, Uji, Japan.

0148-0227/11/2011JA016692

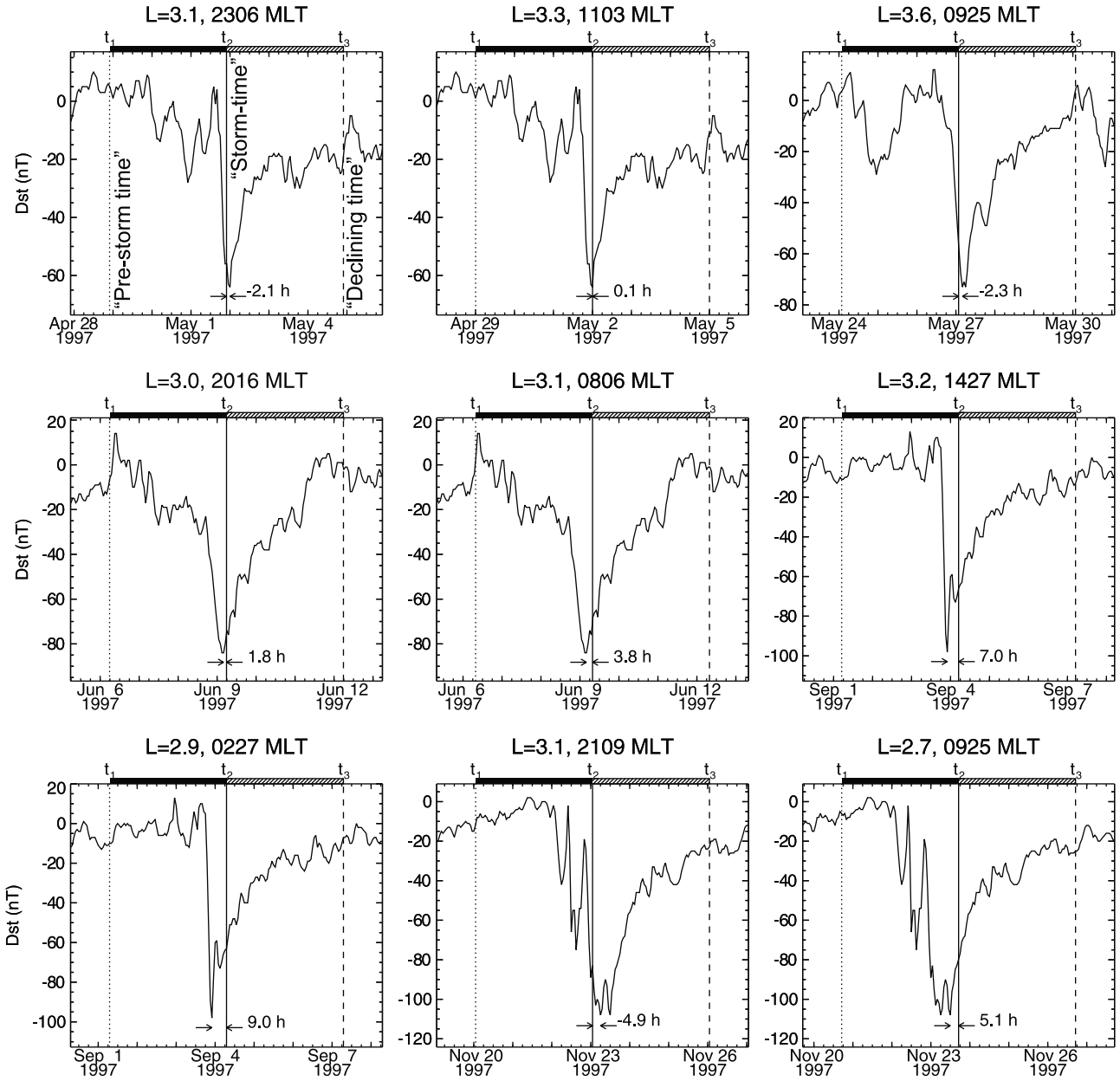

Figure 1. *Dst* indices for the magnetic storms investigated. The *L*-value and MLT of the Polar satellite at t_2 are indicated on the top of each panel. Numerical figure in each panel represents the time difference between t_2 and *Dst* minimum. Vertical dotted, solid, and dashed lines indicate t_1, t_2, and t_3, respectively.

flux can be understood as a combination the betatron and Fermi acceleration. Their result implies that the storm time variation of H^+ depend entirely on pitch angle.

[5] *Fu et al.* [2001] have suggested that diffusive radial transport could have caused the gradual increase in the ions with energy greater than 100 keV during the storm recovery phase. If the diffusive radial transport is the case, the enhancement of H^+ flux will occur at almost all the magnetic local times (MLTs). If the charge exchange, which is the major loss mechanism for the ring current ions, results directly in the decrease in the H^+ flux, the degree of decay will depend on energy. The purpose of this study is to clarify temporal variations of the differential flux of H^+ and its dependence on energy and magnetic local time by means of statistical analysis on the basis of data from the Polar satellite.

2. Data

[6] Polar was launched on 24 February 1996 into an elliptic orbit with its perigee of 2 R_E and apogee of 9 R_E at ~86° inclination [*Acuña et al.*, 1995]. The orbital period of Polar is ~18 h. The Charge and Mass Magnetospheric Ion Composition Experiment/Magnetospheric Ion Composition Sensor (CAMMICE/MICS) aboard the Polar satellite had measured major ionic species, including H^+, O^+, He^+, and He^{++} [*Wilken et al.*, 1992; *Chen et al.*, 1997; *Roeder et al.*,

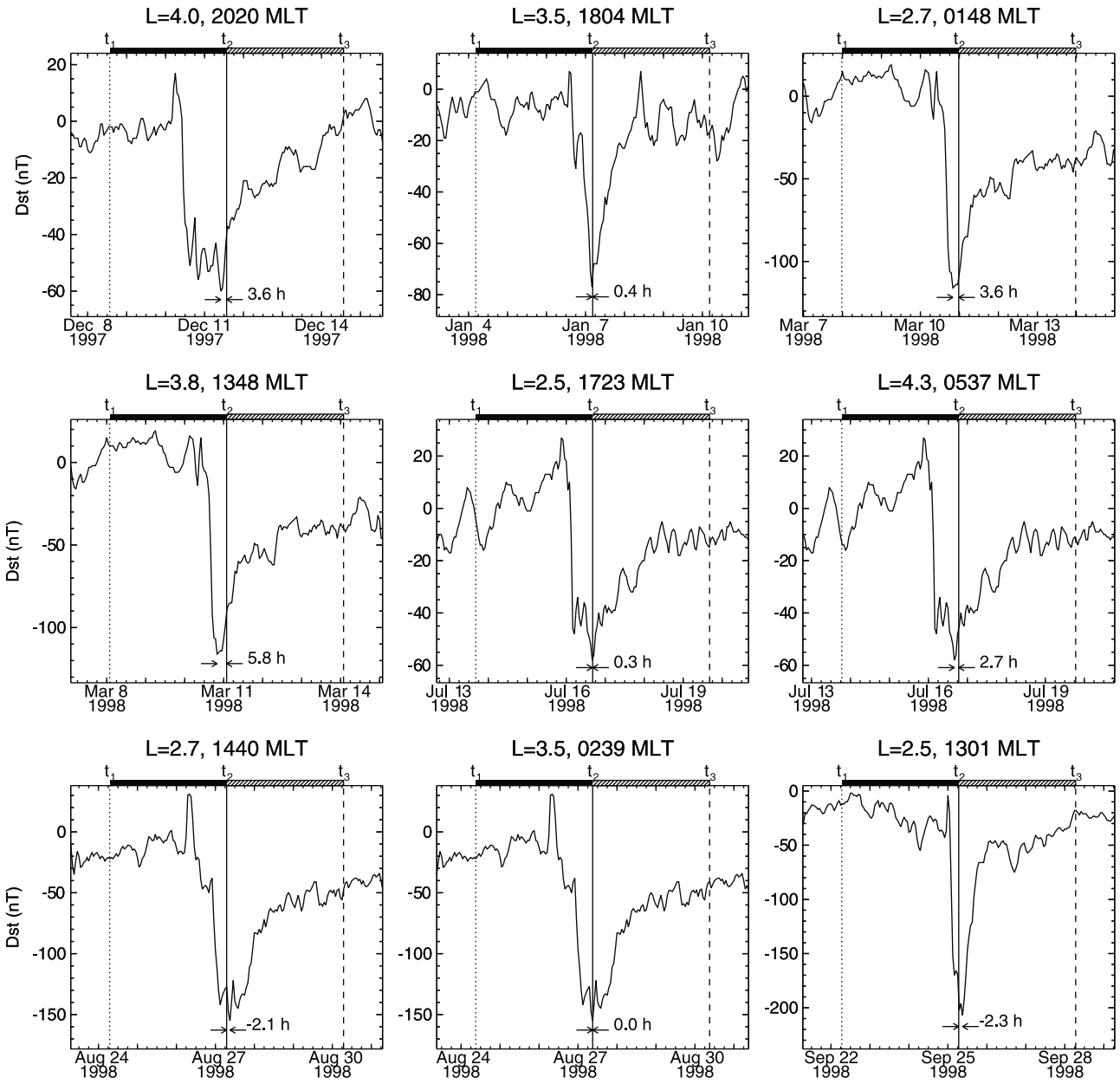

Figure 1. (continued)

2005]. We focus on the differential number fluxes of H^+ in two energy ranges of 31–80 keV and 125–173 keV. Hereafter, we refer to these as low- and high-energy H^+, respectively. H^+ ions having a pitch angle of 90° in the magnetic equatorial plane are investigated to remove the uncertainty arising from the derivation of the second adiabatic invariant. The second adiabatic invariant is a function of the length between two mirror points, but the length cannot be measured by a single satellite. A magnetic field model may give the length, but there remains uncertainty, in particular, during magnetic storms when the magnetic field is largely distorted. To avoid this uncertainty, we focused only on equatorially mirroring H^+. We also used data from the Polar magnetic field investigation (MFI) [*Russell et al.*, 1995] to compare the storm time variation of H^+ with the magnetic field on the equatorial plane.

[7] We selected magnetic storms that satisfy the following three criteria: (1) A storm having its minimum *Dst* index < −50 nT, (2) *Dst* monotonically increasing during the recovery phase, and (3) an isolated storm occurring 3 days or more apart from the other storm. The following terms are used in this paper.

[8] 1. t_2 is the moment at which Polar passed through the magnetic equatorial plane within ±9 h from the time of minimum *Dst* during a storm. t_2 is referred to as the *storm time*.

[9] 2. t_1 is 72 h prior to t_2, and prior to the beginning of the storm. Thus, it is reasonable to call t_1 the *pre-storm time*. Only

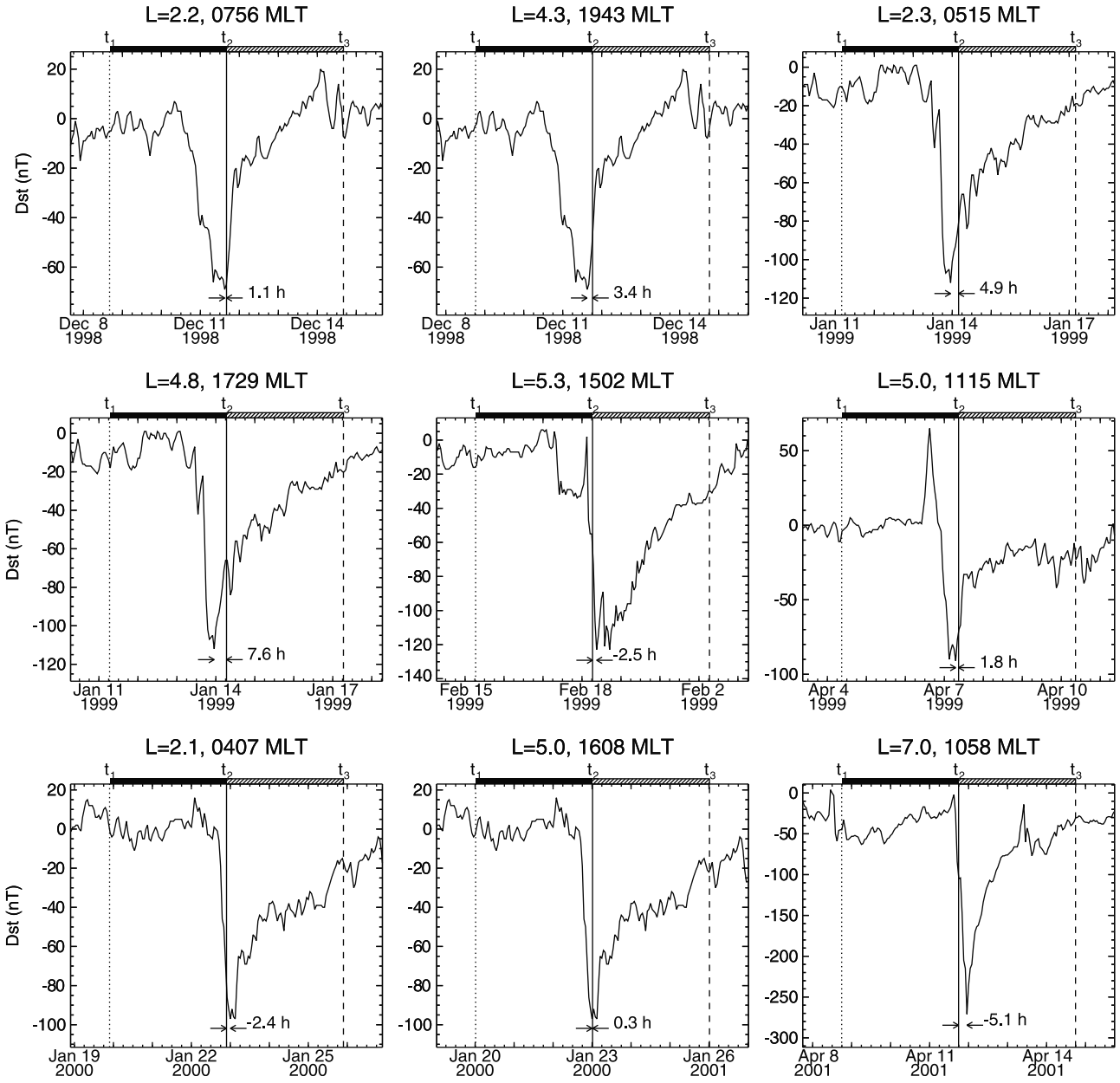

Figure 1. (continued)

the storms satisfying the condition that $Dst(t_1) > Dst(t_2)$ are selected. The Earth's rotation period is 24 h and the Polar's orbital period is around 18 h. Polar returns to almost the same position in the SM coordinates every 72 h with a small displacement of ~3° in magnetic longitude. This choice enables us to minimize the spatial variation.

[10] 3. t_3 is 72 h after t_2. Only the storms satisfying the condition that $Dst(t_3) > Dst(t_2)$ are selected. It is reasonable to call t_3 the *declining time*.

[11] 4. Since $Dst(t_2) < Dst(t_1)$, the ring current is most likely stronger at t_2 than at t_1. We call the interval between t_1 and t_2 the *developing phase*.

[12] 5. Since $Dst(t_3) > Dst(t_2)$, the ring current is most likely weaker at t_3 than at t_2. We call the interval between t_2 and t_3 the *declining phase*.

[13] Hereinafter, subscripts 1, 2, and 3 are used to represent the quantities obtained at t_1, t_2, and t_3, respectively. Twenty-seven pairs of developing-and-declining phases were selected from 6 March 1997 to 17 March 2000 and from 2 April 2001 to 30 April 2002. *Dst* indices for all the pairs are summarized in Figure 1. The Polar satellite encountered the equatorial plane twice in each orbit. Two pairs can be identified in one storm at different MLTs. As is shown in Figure 1, t_1 and t_3 belong to quiet time.

3. Statistical Analysis

3.1. Flux Variation of Low-Energy (31–80 keV) H^+

[14] Figure 2 shows the differential flux variations of H^+ at 31–80 keV during the developing phase (left) and the

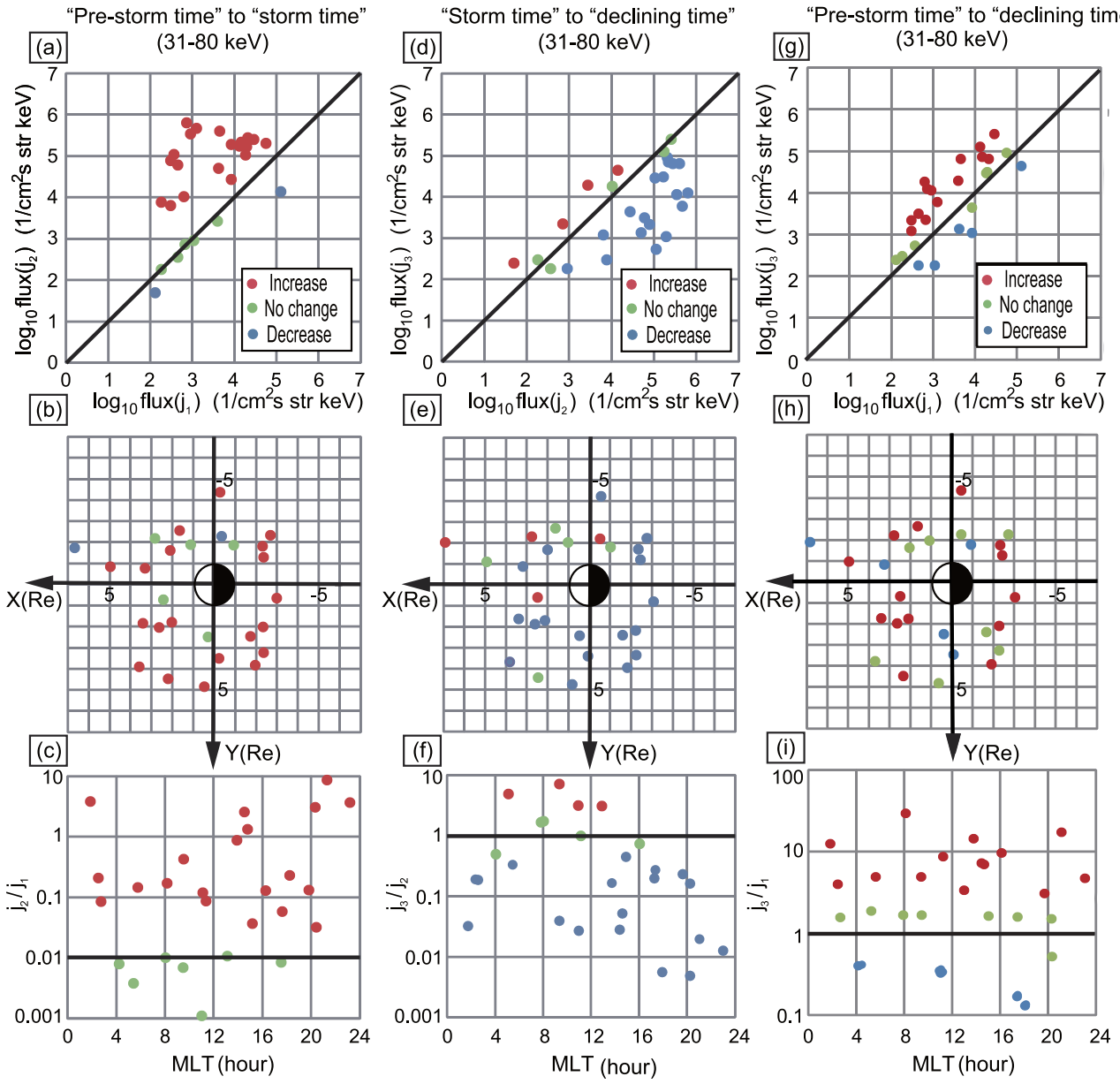

Figure 2. Statistical results for low-energy (31–80 keV) H^+ flux variation for three intervals between t_1 and t_2 (left; developing phase), t_2 and t_3 (middle; declining phase), and t_1 and t_3 (right; "pre-storm time" to "declining time"). (a, d, and g) The differential flux variation. (b, e, and h) Observation locations in the MLT-L coordinates. (c, f, and i) The flux ratio as a function of MLT.

declining phase (right). In Figure 2a, the relationship between the differential flux at the pre-storm time (j_1) and that at the storm time (j_2) is presented. We see that 74% of them increase by a factor of 2 or more (indicated by red color), and 7% of them decrease by a factor of 2 or more (indicated by blue color). Figure 2b shows observation points in the MLT and L coordinates. There is a tendency for the flux to increase at all the MLTs, and for a large increase to occur on the nightside. An exception is found at 06–11 MLT, where the flux decreases by a factor of 2 or more for two cases. Figure 2c shows the j_2/j_1 ratio as a function of MLT, indicating a slight dependence on MLT. The j_2/j_1 ratio is maximized in the premidnight sector, and minimized in the prenoon sector.

[15] Figures 2d and 2e are the same as Figures 2a and 2b except for the relationship between the differential flux at the storm time (j_2) and that at the declining time (j_3). Evidently, 66% of them decrease by a factor of 2 or more (blue), and 15% of them increase by a factor of 2 or more (red). The j_3/j_2 ratio (Figure 2f) is maximized in the prenoon sector and minimized in the premidnight sector. The flux variation shows opposite tendencies between the developing phase and the declining phase. There is no significant difference between the fluxes at t_1 and t_3 as shown in Figure 2i. This means that the flux tends to be recovered to the pre-storm level after storms.

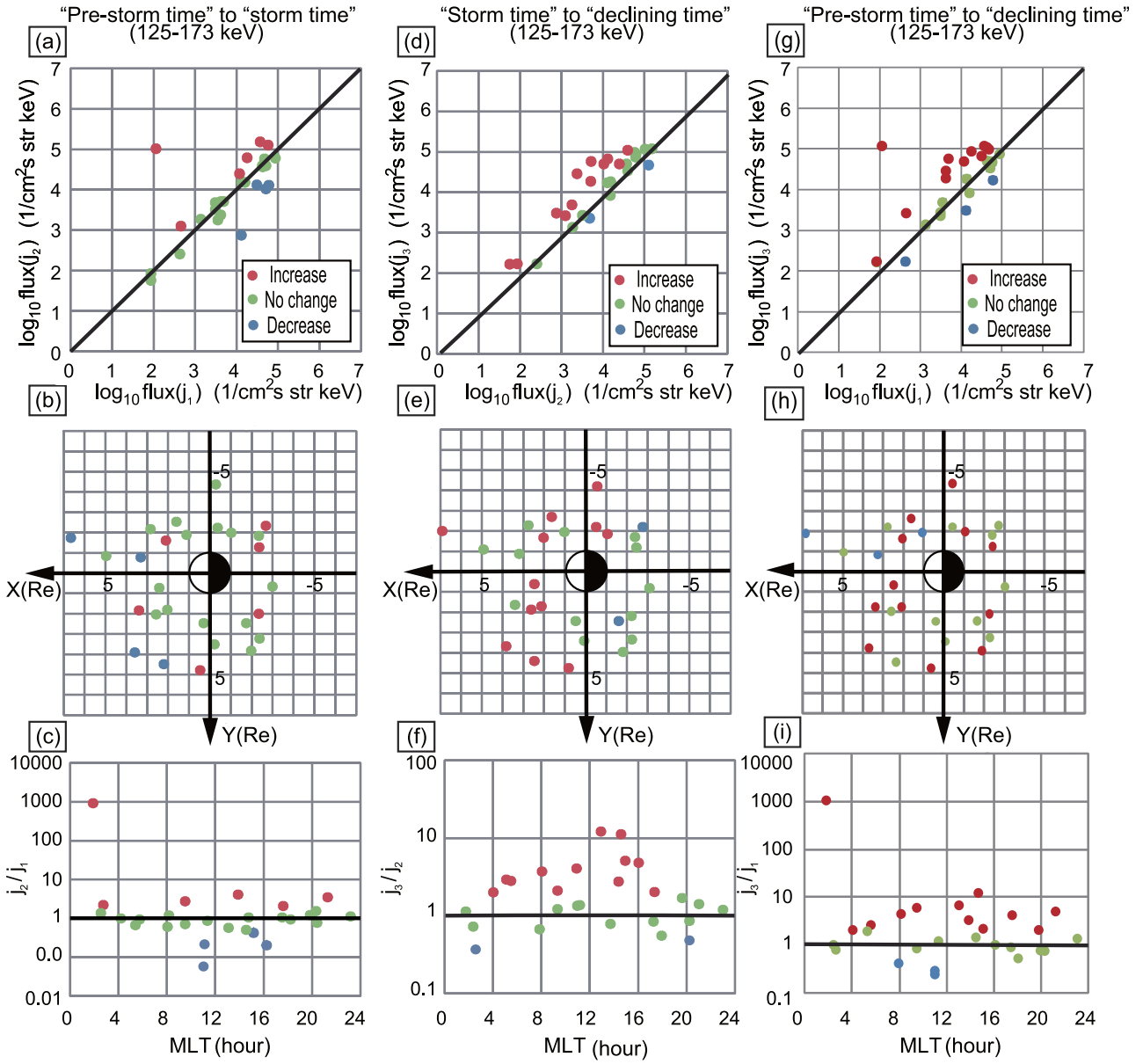

Figure 3. Statistical results for high-energy (125–173 keV) H^+ flux variations. The format is the same as that of Figure 2.

3.2. Flux Variation of High-Energy (125 –173 keV) H^+

[16] Figure 3 is the same as Figure 2 except for the high-energy H^+ at 125–173 keV. The temporal variation of the high-energy H^+ differs completely from that of the low-energy H^+. First, during the developing phase (Figure 3, left), the flux does not change significantly. The deviation of the j_2/j_1 ratio of the high-energy H^+ is much smaller than that of the low-energy H^+. Second, during the declining phase (Figure 3, middle), almost half of them (44%) increase with a factor of 2 or more primarily on the dayside. Third, the flux tends not to be recovered to the pre-storm level as shown in Figure 3i.

3.3. Magnetic Field Variation

[17] Figure 4 shows the magnetic field variation simultaneously observed with the H^+ flux on the equatorial plane. The format of this figure is essentially the same as that of Figures 2 and 3. During the developing phase (Figure 4, left), 59% of them decrease by a factor of 1.1 or more (as indicated by blue). There is a tendency for the magnetic field to significantly decrease on the duskside. During the declining phase (Figure 4, middle), 44% of them increase by a factor of 1.1 or more (indicated by red). 63% of them are unchanged, or recovered to the pre-storm level after storms as shown in Figure 4i.

3.4. Relationship Between Magnetic Field and H^+ Flux Variations

[18] Figure 5 shows the relationship between the magnetic field variations ($\Delta B_{21} \equiv B_2 - B_1$ and $\Delta B_{32} \equiv B_3 - B_2$) and differential flux variations ($\Delta j_{21} \equiv j_2 - j_1$ and $\Delta j_{32} \equiv j_3 - j_2$) of H^+ at 31–80 keV (top) and at 125–173 keV (bottom). The red

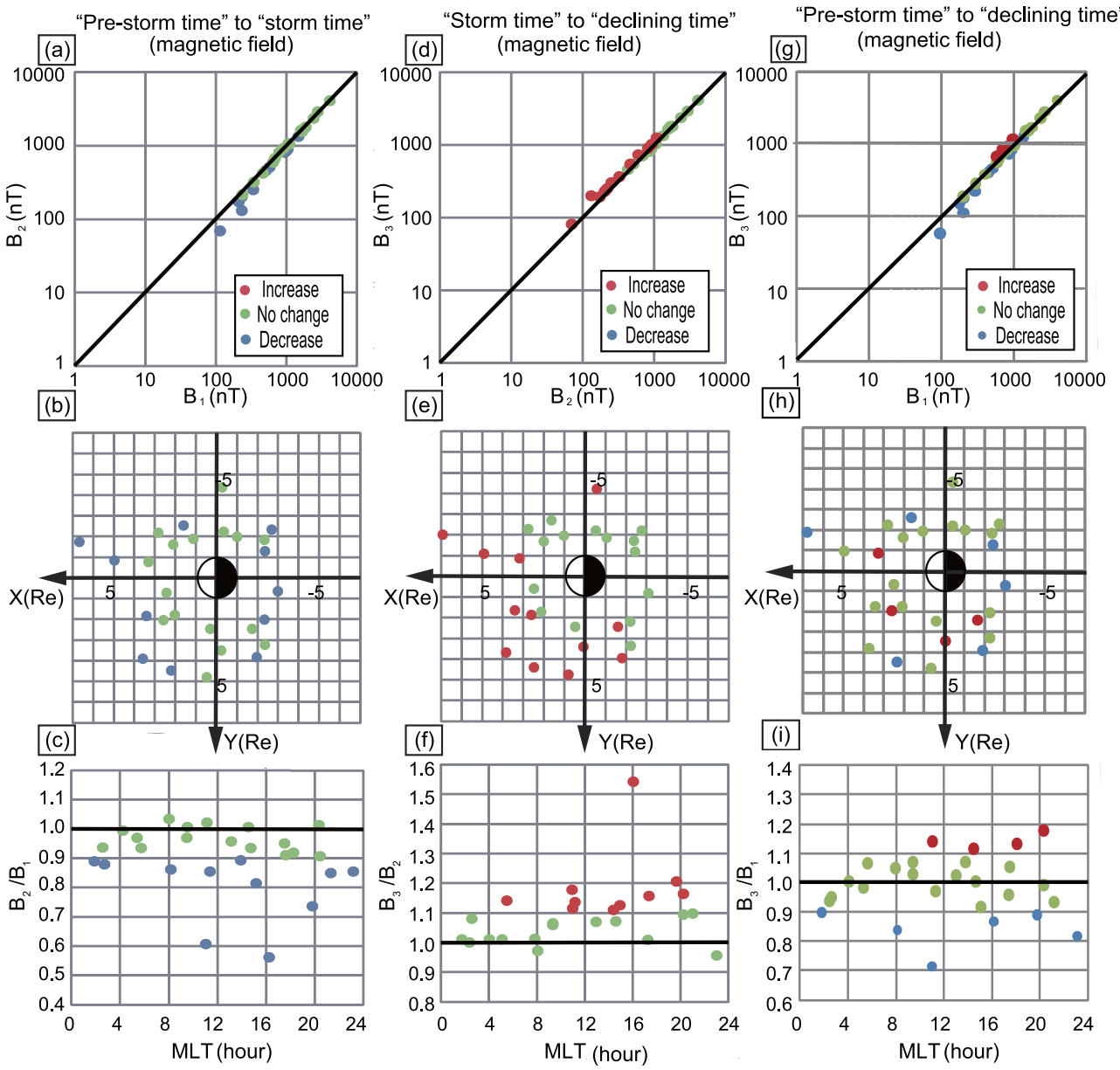

Figure 4. Statistical results for magnetic field variations. The format is the same as that of Figure 2.

color indicates "dayside" and blue, "nightside." A solid circle denotes the variations during the developing phase and an open circle, those during the declining phase. Figure 5 (top) shows that ΔB_{21} and ΔB_{32} tend to decrease with increasing Δj_{21} and Δj_{32}, respectively, at 31–80 keV. That is, the differential flux variation at 31–80 keV is fairly well anti-correlated with the magnetic field variation. As shown in Figure 5 (bottom), there is no clear correlation between the differential flux variation 125–173 keV and the magnetic field variation.

4. Discussion

4.1. Implication of Low-Energy (31–80 keV) H^+ Variation

[19] During the developing phase, the differential H^+ flux at 31–80 keV largely increased on the nightside (14–02 MLT), whereas the flux episodically decreased on the dayside (06–11 MLT). The opposite tendency was observed during the declining phase. This is consistent with the previous statistical study on the storm time variation of the energy density of H^+ [*Ebihara et al.*, 2002] and can be reasonably explained by the increase and decrease in the strength of the convection electric field. The possible explanation is as follows.

[20] The magnetospheric convection electric field is intensified in the magnetosphere by the reconnection process at the dayside magnetopause between the Earth's magnetic field and southward interplanetary magnetic field [e.g., *Dungey*, 1961]. During the storm main phase, the polar cap potential is known to be enhanced [e.g., *Burke et al.*, 2007]. Magnetospheric particles are transported sunward from the nightside plasma sheet by the $\mathbf{E} \times \mathbf{B}$ drift under the enhanced convection electric field. When the magnetic moment ($\mu = W_\perp/B$, where

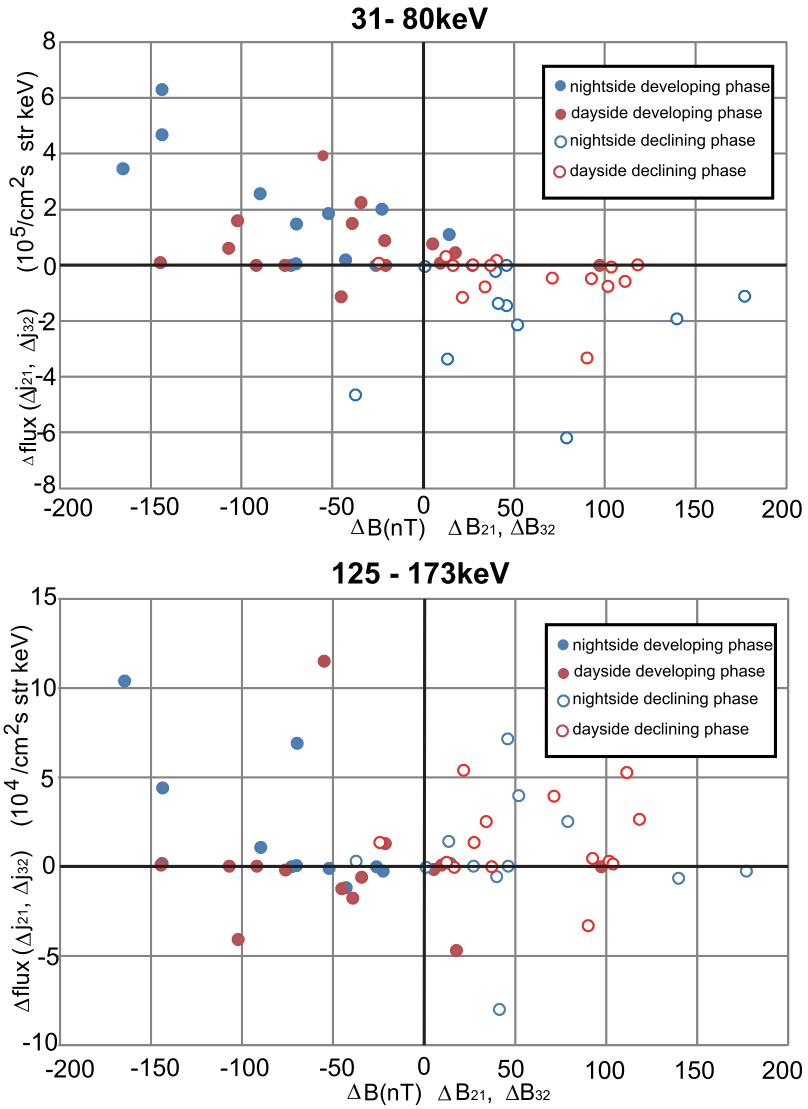

Figure 5. Correlation between the magnetic field variations ($\Delta B_{21} \equiv B_2 - B_1$ or $\Delta B_{32} \equiv B_3 - B_2$) and differential flux variations ($\Delta j_{21} \equiv j_2 - j_1$ or $\Delta j_{32} \equiv j_3 - j_2$) of (top) 31–80 keV H^+ and (bottom) 125–173 keV H^+. The red color indicates "dayside," and the blue color "nightside." Solid circles denote ΔB_{21} and Δj_{21} (developing phase), and circles ΔB_{32} and Δj_{32} (declining phase).

$W_\perp$ is the kinetic energy perpendicular to the magnetic field) is conserved, the particles are adiabatically accelerated as they drift into the region where the magnitude of the magnetic field is strong. As they gain kinetic energy, the gradient-B and curvature drifts become effective. Therefore, H^+ ions tend to move westward, and the flux of H^+ ions increases first on the nightside [*Stüdemann et al.*, 1987; *Korth et al.*, 2000; *Ebihara et al.*, 2002]. The flux of H^+ ions decreased in the dawn-noon sector because the ions flow out through the dayside magnetopause by the enhanced sunward $\mathbf{E} \times \mathbf{B}$ drift velocity [*Ebihara et al.*, 2002]. *Brandt et al.* [2002] have observed an abrupt increase (decrease) in the energetic neutral atoms at 16–50 keV on the nightside (dayside) when the IMF turned southward. When the magnetospheric convection electric field is weakened, the supply of the ions into the inner magnetosphere is suppressed. The ions tend to drift westward due to the gradient-B and curvature drifts with some loss processes including charge exchange. As a consequence, the flux of H^+ ions decreases on the nightside due to loss and increases on the dayside due to azimuthal drift [*Ebihara et al.*, 2002]. The flux can decrease rapidly within 3 days because the e-folding time scale for the charge exchange loss is ~0.3 (~1.7) days at $L = 3$ ($L = 5$) for 30 keV H^+ [*Fok et al.*, 1991].

[21] The storm time variation of the flux of low-energy H^+ is quite similar to that of the energy density of H^+, as was derived by *Ebihara et al.* [2002]. Low-energy H^+ and the magnetic field are anti-correlated with each other. These two observational facts might imply that the low-energy H^+ is a prime carrier of the storm time proton ring current that inflates the magnetic field in the inner magnetosphere.

4.2. Implication of High-Energy (125–173 keV) H^+ Variation

[22] The storm time variation of the flux of high-energy (125–173 keV) H^+ is different from that of low-energy

(31–80 keV) H^+. This implies that the high-energy H^+ flux variation is not simply explained in terms of the strength of the convection electric field. During the main phase of large magnetic storms, the polar cap potential can increase to ~200 kV [*Burke et al.*, 2007]. Thus, the high-energy particles (125–173 keV) may gain kinetic energy as they drift in the inner magnetosphere. *Lyons and Williams* [1976] have shown that H^+ at 164 keV indicates no significant response to the magnetic storm of December 1971 at L = 4–5 when viewed at constant energy, whereas H^+ shows a significant intensity increase when viewed at constant μ. For >200 keV, the H^+ intensity indicates a decrease during the storm main phase when viewed at constant energy, whereas the H^+ intensity remains constant when viewed at constant μ. This implies that the increase in high-energy H^+ could have been suppressed by adiabatic deceleration under the influence of the reduced (inflated) magnetic field. For >200 keV, the influence of the reduction (inflation) of the magnetic field dominates the increase in H^+, resulting in a decrease in the H^+ flux. Unfortunately, MICS did not measure the ions with energy >200 keV.

[23] During the declining phase, there is a tendency for the high-energy H^+ flux to increase, in particular, on the dayside, as shown in Figure 3f. The flux enhancements are hardly explained by the reduction of the convection electric field. There are at least five possible mechanisms leading to flux enhancements of the high-energy H^+.

[24] First, the high-energy H^+ could have been adiabatically accelerated due to the increase in the ambient magnetic field intensity caused by the weakening of the ring current. When the magnetic moment (μ) is conserved, the perpendicular energy ($W_\perp$) of H^+ is increased by intensification of the magnetic field [*Lyons*, 1977; *Ebihara et al.*, 2008]. This process is referred to as gyrobetatron acceleration. Since the high-energy H^+ is poorly correlated with the magnetic field, the evidence for gyrobetatron acceleration is unavailable.

[25] Second, the high-energy H^+ could have been radially transported by the induction electric field associated with time variation of the magnetic field in the inner magnetosphere. The induction electric field is directed westward during the decline phase because the magnetic field tends to be globally increased in the inner magnetosphere. Therefore, high-energy H^+ can be accelerated as they drift westward, and be displaced inward by the $\mathbf{E} \times \mathbf{B}$ drift. This process is referred to as drift-betatron acceleration, and will be investigated using radial profiles of the phase space density of H^+ as was previously done by *Lui* [1993].

[26] Third, the high-energy H^+ could have been radially transported by diffusion [e.g., *Nakada and Mead*, 1965; *Lyons and Schulz*, 1989; *Fu et al.*, 2001]. If this was the case, the enhancement of high-energy H^+ would occur at all the MLTs. This is inconsistent with the observational fact that the high-energy H^+ tends to increase mainly on the dayside and in the predawn sector during the declining phase. The radial diffusion cannot fully explain the uneven enhancement of the high-energy H^+ flux.

[27] Fourth, the high-energy H^+ could have been accelerated or transported by a substorm [e.g., *Belian et al.*, 1978]. Substorm-associated acceleration of particles has been observed frequently on the nightside at the geosynchronous altitude [e.g., *Birn et al.*, 1997] and at L = 4–8 [e.g., *Friedel et al.*, 1996]. Once injected, the high-energy H^+ will drift azimuthally, and the spatial distribution of it will become close to uniform in azimuth. Thus, the substorm-associated acceleration is unlikely to explain the uneven enhancement of the high-energy H^+.

[28] Fifth, H^+ could have been accelerated by triggered emissions of electromagnetic ion cyclotron (EMIC) waves [*Omura et al.*, 2010; *Shoji and Omura*, 2011]. *Shoji and Omura* [2011] performed a self-consistent one-dimensional hybrid code. According to the results, some H^+ ions are scattered into the loss cone, while some of them with pitch angles near 90° are accelerated by the triggered emission.

[29] The high-energy H^+ undergoes a relatively slow decay. The e-folding time scale for the charge exchange loss for 125 keV H^+ is ~10 (~50) days at L = 3 (L = 5) [*Fok et al.*, 1991]. After the declining phase, some of high-energy H^+ may remain until the beginning of the next storm.

5. Conclusions

[30] One Low-energy (31–80 keV) differential H^+ flux showed a substantial increase and decrease in the inner magnetosphere during the developing and declining phases of magnetic storms, respectively. The opposite tendency was observed in and near the dawn-noon sector. The overall behavior of the low-energy H^+ can be explained in terms of competition between the $\mathbf{E} \times \mathbf{B}$ drift and magnetic drift. The low-energy H^+ flux and the ambient magnetic field were anti-correlated with each other, most likely indicating a diamagnetic nature.

[31] Two storm time variation of high-energy (125–173 keV) H^+ is completely different from that of low-energy H^+. The high-energy H^+ shows the tendency that it increases during the declining phase, in particular, on the dayside. The uneven enhancement of the high-energy H^+ flux is not simply understood in terms of diffusive transport and substorm-associated acceleration. The high-energy H^+ flux and the ambient magnetic field are poorly correlated with each other, suggesting that gyrobetatron acceleration is unlikely. Some other processes, drift-betatron acceleration, or non-adiabatic acceleration, could be predominant in the uneven enhancement of high-energy H^+ flux during the declining phase.

[32] **Acknowledgments.** We used the *Dst* index provided by WDC for Geomagnetism, Kyoto. This work was supported by the Global COE Program of Nagoya University "Quest for Fundamental Principles in the Universe (QFPU)" from JSPS and MEXT of Japan. We thank Theodore A. Fritz and Manuel Grande for providing us the Polar MICS data and valuable discussions, and Christopher T. Russell for the Polar MFE data.

[33] Robert Lysak thanks the reviewers for their assistance in evaluating this paper.

References

Acuña, M. H., et al. (1995), The global geospace science program and its investigations, *Space Sci. Rev.*, *71*, 5–21, doi:10.1007/BF00751323.

Belian, R. D., D. N. Baker, P. R. Higbie, and E. W. Hones Jr. (1978), High-resolution energetic particle measurements at 6.6 RE: 2. High-energy proton drift echoes, *J. Geophys. Res.*, *83*(A10), 4857–4862, doi:10.1029/JA083iA10p04857.

Berko, F., L. Cahill Jr., and T. A. Fritz (1975), Protons as the prime contributors to storm time ring current, *J. Geophys. Res.*, *80*(25), 3549–3552, doi:10.1029/JA080i025p03549.

Birn, J., M. F. Thomsen, J. E. Borovsky, G. D. Reeves, D. J. McComas, and R. D. Belian (1997), Characteristic plasma properties during disper-

sionless substorm injections at geosynchronous orbit, *J. Geophys. Res.*, *102*(A2), 2309–2324, doi:10.1029/96JA02870.
Brandt, P. C., D. G. Mitchell, Y. Ebihara, B. R. Sandel, E. C. Roelof, J. L. Burch, and R. Demajistre (2002), Global IMAGE/HENA observations of the ring current: Examples of rapid response to IMF and ring current-plasmasphere interaction, *J. Geophys. Res.*, *107*(A11), 1359, doi:10.1029/2001JA000084.
Burke, W. J., L. C. Gentile, and C. Y. Huang (2007), Penetration electric fields driving main phase Dst, *J. Geophys. Res.*, *112*, A07208, doi:10.1029/2006JA012137.
Cahill, L. J., Jr. (1966), Inflation of the inner magnetosphere during a magnetic storm, *J. Geophys. Res.*, *71*(19), 4505–4519.
Chen, J., T. A. Fritz, R. B. Sheldon, H. E. Spence, W. N. Spjeldvik, J. F. Fennell, and S. Livi (1997), A new, temporarily confined population in the polar cap during the August 27, 1996 geomagnetic field distortion period, *Geophys. Res. Lett.*, *24*(12), 1447–1450, doi:10.1029/97GL01369.
Dessler, A. J., and R. Karplus (1961), Some effects of diamagnetic ring currents on Van Allen radiation, *J. Geophys. Res.*, *66*(8), 2289–2295, doi:10.1029/JZ066i008p02289.
Dungey, J. W. (1961), Interplanetary magnetic field and the auroral zones, *Phys. Rev. Lett.*, *6*, 47–48, doi:10.1103/PhysRevLett.6.47.
Ebihara, Y., M. Ejiri, H. Nilsson, I. Sandahl, A. Milillo, M. Grande, J. F. Fennell, and J. L. Roeder (2002), Statistical distribution of the storm-time proton ring current: Polar measurements, *Geophys. Res. Lett.*, *29*(20), 1969, doi:10.1029/2002GL015430.
Ebihara, Y., M. Fok, J. B. Blake, and J. F. Fennell (2008), Magnetic coupling of the ring current and the radiation belt, *J. Geophys. Res.*, *113*, A07221, doi:10.1029/2008JA013267.
Fok, M.-C., J. Kozyra, A. Nagy, and T. Cravens (1991), Lifetime of ring current particles due to Coulomb collisions in the plasmasphere, *J. Geophys. Res.*, *96*(A5), 7861–7867, doi:10.1029/90JA02620.
Frank, L. A. (1967), Initial observations of low-energy electrons in Earth's magnetosphere with OGO 3, *J. Geophys. Res.*, *72*(15), 3753–3767, doi:10.1029/JZ072i015p03753.
Friedel, R. H. W., A. Korth, and G. Kremser (1996), Substorm onsets observed by CRRES: Determination of energetic particle source regions, *J. Geophys. Res.*, *101*(A6), 13,137–13,154.
Fu, S. Y., B. Wilken, Q. G. Zong, and Z. Y. Pu (2001), Ion composition variations in the inner magnetosphere: Individual and collective storm effects in 1991, *J. Geophys. Res.*, *106*(A12), 29,683–29,704, doi:10.1029/2000JA900173.
Hoffman, R., and L. Cahill Jr. (1968), Ring current particle distributions derived from ring current magnetic field measurements, *J. Geophys. Res.*, *73*(21), 6711–6722, doi:10.1029/JA073i021p06711.
Korth, A., R. Friedel, C. Mouikis, J. Fennell, J. Wygant, and H. Korth (2000), Comprehensive particle and field observations of magnetic storms at different local times from the CRRES spacecraft, *J. Geophys. Res.*, *105*(A8), 18,729–18,740, doi:10.1029/1999JA000430.
Krimigis, S. M., G. Gloeckler, R. W. McEntire, T. A. Potemra, F. L. Scarf, and E. G. Shelley (1985), Magnetic storm of September 4, 1984: A synthesis of ring current spectra and energy densities measured with AMPTE/CCE, *Geophys. Res. Lett.*, *12*(5), 329–332, doi:10.1029/GL012i005p00329.
Li, X., D. N. Baker, M. Temerin, T. E. Cayton, E. G. D. Reeves, R. A. Christensen, J. B. Blake, M. D. Looper, R. Nakamura, and S. G. Kanekal (1997), Multisatellite observations of the outer zone electron variation during the November 3–4, 1993, magnetic storm, *J. Geophys. Res.*, *102*(A7), 14,123–14,140, doi:10.1029/97JA01101.
Liu, S., M. W. Chen, J. L. Roeder, L. R. Lyons, and M. Schulz (2005), Relative contribution of electrons to the stormtime total ring current energy content, *Geophys. Res. Lett.*, *32*, L03110, doi:10.1029/2004GL021672.
Lui, A. T. Y. (1993), Radial transport of storm time ring current ions, *J. Geophys. Res.*, *98*(A1), 209–214, doi:10.1029/92JA02079.
Lui, A., R. McEntire, and S. Krimigis (1987), Evolution of the ring current during two geomagnetic storms, *J. Geophys. Res.*, *92*(A7), 7459–7470, doi:10.1029/JA092iA07p07459.
Lyons, L. R. (1977), Adiabatic evolution of trapped particle pitch angle distributions during a storm main phase, *J. Geophys. Res.*, *82*(16), 2428–2432, doi:10.1029/JA082i016p02428.
Lyons, L., and M. Schulz (1989), Access of energetic particles to storm time ring current through enhanced radial "diffusion," *J. Geophys. Res.*, *94*(A5), 5491–5496, doi:10.1029/JA094iA05p05491.
Lyons, L., and D. Williams (1976), Storm-associated variations of equatorially mirroring ring current protons, 1–800 keV, at constant first adiabatic invariant, *J. Geophys. Res.*, *81*(1), 216–220, doi:10.1029/JA081i001p00216.
McIlwain, C. E. (1966), Ring current effects on trapped particles, *J. Geophys. Res.*, *71*(15), 3623–3628.
Nakada, M. P., and G. D. Mead (1965), Diffusion of protons in the outer radiation belt, *J. Geophys. Res.*, *70*(19), 4777–4791, doi:10.1029/JZ070i019p04777.
Omura, Y., J. Pickett, B. Grison, O. Santolik, I. Dandouras, M. Engebretson, P. M. E. Décréau, and A. Masson (2010), Theory and observation of electromagnetic ion cyclotron triggered emissions in the magnetosphere, *J. Geophys. Res.*, *115*, A07234, doi:10.1029/2010JA015300.
Roeder, J. L., M. W. Chen, J. F. Fennell, and R. Friedel (2005), Empirical models of the low-energy plasma in the inner magnetosphere, *Space Weather*, *3*, S12B06, doi:10.1029/2005SW000161.
Russell, C. T., R. C. Snare, J. D. Means, D. Pierce, D. Dearborn, M. Larson, G. Barr, and G. Le (1995), The GGS/Polar magnetic fields investigation, *Space Sci. Rev.*, *71*, 563–582, doi:10.1007/BF00751341.
Shoji, M., and Y. Omura (2011), Simulation of electromagnetic ion cyclotron triggered emissions in the Earth's inner magnetosphere, *J. Geophys. Res.*, *116*, A05212, doi:10.1029/2010JA016351.
Shprits, Y. Y., R. M. Thorne, R. Friedel, G. D. Reeves, J. Fennell, D. N. Baker, and S. G. Kanekal (2006), Outward radial diffusion driven by losses at magnetopause, *J. Geophys. Res.*, *111*, A11214, doi:10.1029/2006JA011657.
Smith, P. H., and R. A. Hoffman (1973), Ring current particle distributions during the magnetic storms of December 16–18, 1971, *J. Geophys. Res.*, *78*(22), 4731–4737, doi:10.1029/JA078i022p04731.
Smith, P., and R. Hoffman (1974), Direct observations in the dusk hours of the characteristics of the storm time ring current particles during the beginning of magnetic storms, *J. Geophys. Res.*, *79*(7), 966–971, doi:10.1029/JA079i007p00966.
Stüdemann, W., et al. (1987), The May 2–3, 1986 magnetic storm: First energetic ion composition observations with the Mics instrument on Viking, *Geophys. Res. Lett.*, *14*(4), 455–458, doi:10.1029/GL014i004p00455.
Wilken, B., et al. (1992), Magnetospheric ion composition spectrometer onboard the CRRES spacecraft, *J. Spacecr. Rockets*, *29*(4), 585–591, doi:10.2514/3.25503.
Williams, D. J. (1981), Ring current composition and sources: An update, *Planet. Space Sci.*, *29*, 1195–1203, doi:10.1016/0032-0633(81)90124-0.
Williams, D. J. (1987), Ring current and radiation belts, *Rev. Geophys.*, *25*, 570–578, doi:10.1029/RG025i003p00570.
Williams, D., J. Arens, and L. Lanzerotti (1968), Observations of trapped electrons at low and high altitudes, *J. Geophys. Res.*, *73*(17), 5673–5696, doi:10.1029/JA073i017p05673.
Zaharia, S., M. F. Thomsen, J. Birn, M. H. Denton, V. K. Jordanova, and C. Z. Cheng (2005), Effect of storm-time plasma pressure on the magnetic field in the inner magnetosphere, *Geophys. Res. Lett.*, *32*, L03102, doi:10.1029/2004GL021491.

Y. Ebihara, Research Institute for Sustainable Humanosphere, Kyoto University, Uji 611-0011, Japan. (ebihara@rish.kyoto-u.ac.jp)
A. Temporin, Solar-Terrestrial Environment Laboratory, Nagoya University, Nagoya 464-8601, Japan.